

D. CAVOURAS<sup>1</sup>  
I. KANDARAKIS<sup>1</sup>, ✉  
D. NIKOLOPOULOS<sup>1</sup>  
I. KALATZIS<sup>1</sup>  
G. KAGADIS<sup>2</sup>  
N. KALIVAS<sup>3</sup>  
A. EPISKOPAKIS<sup>1</sup>  
D. LINARDATOS<sup>1</sup>  
M. ROUSSOU<sup>1</sup>  
E. NIRGIANAKI<sup>1</sup>  
D. MARGETIS<sup>1</sup>  
I. VALAIS<sup>1</sup>  
I. SIANOUDIS<sup>4</sup>  
K. KOURKOUTAS<sup>4</sup>  
N. DIMITROPOULOS<sup>5</sup>  
A. LOUIZI<sup>6</sup>  
C. NOMICOS<sup>7</sup>  
G. PANAYIOTAKIS<sup>2</sup>

# Light emission efficiency and imaging performance of $Y_3Al_5O_{12}: Ce$ (YAG: Ce) powder screens under diagnostic radiology conditions

<sup>1</sup>Department of Medical Instrumentation Technology, Technological Educational Institution of Athens, 122 10 Athens, Greece

<sup>2</sup>Department of Medical Physics, Medical School, University of Patras, 265 00 Patras, Greece

<sup>3</sup>Greek Atomic Energy, Commission P.O. BOX 60092, 15310, Agia Paraskevi, Greece

<sup>4</sup>Department of Physics, Chemistry and Materials Technology, Technological Educational Institution of Athens, 122 10 Athens, Greece

<sup>5</sup>Department of Medical Imaging, Euromedica Medical Center, 2 Mesogeion Ave., Athens, Greece

<sup>6</sup>Laboratory of Medical Physics, University of Athens, Greece

<sup>7</sup>Department of Electronics, Technological Educational Institution of Athens, 122 10 Athens, Greece

Received: 4 November 2004 /

Revised version: 13 February 2005

Published online: 22 April 2005 • © Springer-Verlag 2005

**ABSTRACT** In this study  $Y_3Al_5O_{12}: Ce$  powder scintillator was evaluated for use in X-ray imaging detectors. This phosphor, also known as YAG: Ce scintillator or P-46 phosphor, is a non-hygroscopic, emitting green light with very short decay time. These properties are very attractive for X-ray imaging.  $Y_3Al_5O_{12}: Ce$  powder was used to prepare various test screens (33–166 mg/cm<sup>2</sup>). Absolute luminescence efficiency measurements were performed for various X-ray tube voltages (50–130 kVp). In addition parameters related to image quality such as the modulation transfer function and the detective quantum efficiency were examined. A theoretical model, describing radiation and light transfer, was employed to fit experimental data and to estimate values of optical parameters. Absolute efficiency was found to decrease with X-ray tube voltage. Highest efficiency was obtained for the 107 mg/cm<sup>2</sup> screen. Light attenuation coefficients were close to those of green emitting rare earth scintillators. At low spatial frequencies the detective quantum efficiency was high for the 107–166 mg/cm<sup>2</sup> screens. The light emission efficiency and imaging performance of  $Y_3Al_5O_{12}: Ce$  was not better than currently employed scintillators. However due to its very fast response and high spectral compatibility to optical sensors it may be considered for use in digital imaging detectors.

PACS 07.85; 42.30; 42.80

## 1 Introduction

Scintillators, or phosphors, coupled to optical sensors (photodiodes, photocathodes, films etc) are employed in most radiation detectors used in medical imaging systems [1–3]. Cerium ( $Ce^{3+}$ ) doped scintillators are of particular interest for medical imaging, because of their very fast response. The latter is due to a  $4f - 5d$  electric dipole transition in Ce ion [4, 5].

In this study  $Y_3Al_5O_{12}: Ce$  (cerium doped yttrium aluminum oxide or yttrium aluminate) powder scintillator was examined under exposure conditions employed in diagnostic medical radiology. This material, also known as YAG: Ce (yttrium–aluminum garnet) scintillator or P-46 phosphor, is non-hygroscopic, emitting green light (530–550 nm) with very short decay time (68 ns) [6–12]. These properties are very attractive for X-ray imaging since: (i) green light shows high spectral compatibility with a large number of existing optical sensors (amorphous or crystalline silicon photodiodes, charge coupled devices, photocathodes, ortho-chromatic films), (ii) fast decay time is a prerequisite for dynamic real-time imaging.

$Y_3Al_5O_{12}: Ce$  has been previously studied for various, mainly non-imaging, radiation detection applications [8–13]. In most of these applications  $Y_3Al_5O_{12}: Ce$  has been employed in single-crystal form or in the form of transparent optical ceramic [8–12]. Powder  $Y_3Al_5O_{12}: Ce$  phosphor has also been studied for use in X-ray detectors employed in hot plasma fusion facilities [14]. In a recent study of our group [15], data on the  $Y_3Al_5O_{12}: Ce$  scintillator were reported mainly concerning intrinsic properties such as X-ray absorption, intrinsic X-ray to light conversion, emitted spectrum and spectral compatibility to optical sensors.

In the present study the imaging properties of  $Y_3Al_5O_{12}: Ce$  scintillator, were systematically investigated. This was

accomplished by experimental and theoretical evaluation of various parameters related to image brightness, image resolution and signal to noise ratio. The scintillator was used in the form of screens (layers) of various thickness and the parameters investigated were the absolute efficiency (AE), the X-ray luminescence efficiency (XLE), the modulation transfer function (MTF), the noise power spectrum (NPS) and the detective quantum efficiency (DQE) [14–25].

## 2 Materials and methods

### 2.1 Output signal and signal transfer efficiency

The output signal of a scintillating screen may be expressed by either the emitted light energy fluence- $\Psi_\Lambda$  (light energy per unit of area) or the emitted light photon fluence- $\Phi_\Lambda$  (light photons per unit of area) [19–21]:

$$\Psi_\Lambda(E_0) = \int_0^{E_0} \psi_0(E) \eta_e(E) \eta_C g_\Lambda(E, \sigma, \tau) dE \quad (1)$$

$$\Phi_\Lambda(E_0) = \int_0^{E_0} \phi_0(E) \eta_Q(E) m_\lambda(E) g_\Lambda(E, \sigma, \tau) dE \quad (2)$$

where  $\psi_0(E)$  is the incident X-ray energy fluence spectral distribution (energy fluence per energy interval) and  $\phi_0(E)$  is the incident X-ray photon fluence spectral distribution (photon fluence per energy interval).  $E$  is the X-ray photon energy and  $E_0$  is the maximum energy of the X-ray spectrum.  $\eta_s(E)$  is the energy absorption efficiency (EAE), which is the fraction of incident X-ray energy absorbed by the scintillator.  $\eta_Q(E)$  is the quantum detection efficiency (QDE), being the fraction of the total number of incident X-ray quanta interacting in the scintillator.  $\eta_C$  is the intrinsic X-ray to light conversion efficiency expressing the fraction of absorbed X-ray energy converted into light energy within the screen material.  $m_\lambda(E)$  is the intrinsic quantum conversion gain, i.e., the number of light quanta generated within the scintillator per X-ray absorbed.  $g_\Lambda$  is the light transmission efficiency, expressing the fraction of light escaping the scintillator. This fraction may be described in terms of the optical attenuation coefficients  $\sigma$ ,  $\tau$  [15–18]. The light energy fluence and the light photon fluence were modeled by suitably modifying previously published theoretical models [17, 18, 20]. Details on the specific expressions and calculations of all the aforementioned quantities are given in the appendix and in Refs. [14, 16–18, 20].

The efficiency of a scintillating screen to transfer the signal from the input to the output is expressed by the X-ray luminescence efficiency -XLE, ( $\eta_\psi$ ). XLE is defined as the ratio of the emitted light energy fluence over the incident X-ray energy fluence: ( $\eta_\psi = \Psi_\Lambda / \Psi_0$ ) [16, 17, 20]. For monoenergetic radiation  $\eta_\psi$  may be determined by the product  $\eta_e(E) \eta_C g_\Lambda(E, \sigma, \tau)$ . To be consistent with experimental conditions the X-ray luminescence efficiency is often expressed through the ratio of emitted light energy fluence,  $\Psi_\Lambda$ , over the incident exposure  $X$ . This ratio has been previously referred to as the absolute efficiency-AE, ( $\eta_A$ ) [14, 16]:

$$\eta_A = \Psi_\Lambda(E_0) / X \quad (3)$$

In most cases it is of interest to examine the efficiency of a scintillating screen with respect to its combination with a certain optical sensor (photodiode, photocathode, film etc). In such cases the effective luminescence efficiency-EE ( $\eta_{\text{eff}}$ ) is used. EE was defined by the relation:  $\eta_{\text{eff}} = \eta_\psi c_s$ , where  $c_s$  is the spectral compatibility factor expressing the compatibility of the scintillator's emission spectrum to the spectral sensitivity of the optical sensor (see relation (12) in Sect. 2.4)

To describe the imaging properties and contrast and spatial resolution of a scintillating screen, the signal transfer efficiency is often expressed by the modulation transfer function (MTF)- $M$  [18–22, 24, 25]. MTF is used in the evaluation of imaging systems in the Fourier domain, assuming that systems considered are linear. It is widely accepted, however, that scintillating screens are compatible with linear systems theory assumptions [26].

MTF has been defined as the spatial frequency-dependent output signal (photon fluence) normalized to zero frequency, as follows:

$$M(E_0, \nu) = \Phi_\Lambda(E_0, \nu) / \Phi_\Lambda(E_0, \nu = 0) \quad (4)$$

where  $\nu$  denotes spatial frequency. Hence the output signal may be expressed in the spatial frequency domain in terms of MTF:

$$\begin{aligned} \Phi_\Lambda(E_0, \nu) \\ = M(E_0, \nu) \left[ \int_0^{E_0} \phi_0(E) \eta_Q(E) m_\lambda(E) g_\Lambda(E, \sigma, \tau) dE \right] \end{aligned} \quad (5)$$

### 2.2 Output noise and noise transfer

The output noise of a scintillating screen is expressed by the variance in the emitted light photon fluence (number of photons per unit of area) over the screen emitting area. In the spatial frequency domain noise is expressed by the noise power spectrum (NPS)- $W$  [19–23]. The latter may be obtained by the Fourier transform of data obtained after uniform irradiation of the screens [19, 22, 23]. NPS has been also expressed in terms of  $\eta_Q$ ,  $m_\lambda$ ,  $g_\Lambda$  [23].

### 2.3 Signal to noise ratio and detective quantum efficiency

The detective quantum efficiency ( $\eta_D(\nu)$ ) of a scintillating screen has been defined by the relation  $\eta_D = \text{SNR}_{\text{out}}^2 / \text{SNR}_{\text{in}}^2$  [22]. In this relation  $\text{SNR}_{\text{out}}$  is the output signal to noise ratio of a scintillating screen whereas  $\text{SNR}_{\text{in}}$  is the input signal to noise ratio. In the spatial frequency domain the square of the output signal may be obtained using relations (4) and (2). The square of the output noise is given by the noise power spectrum  $W(E_0, \nu)$  [22, 23]. Hence DQE may be written as follows:

$$\eta_D(\nu) = \frac{(\Phi_\Lambda(E_0) M(E_0, \nu))^2}{W(E_0, \nu) \text{SNR}_{\text{in}}^2} \quad (6)$$

The emitted light photon fluence,  $\Phi_{\Lambda}(E_0)$  may be expressed in terms of experimentally measurable quantities (absolute efficiency, exposure, mean light wavelength) using the relation:

$$\Phi_{\lambda} = (\eta_{\Lambda} X) / hc\bar{\lambda}^{-1} \quad (7)$$

Where the numerator is equal to the light energy fluence ( $\Psi_{\Lambda} = \eta_{\Lambda} X$ ) and the denominator is equal to the mean energy ( $E_{\lambda}$ ) of the emitted light photons ( $E_{\lambda} = hc/\bar{\lambda}$ ),  $\bar{\lambda}$  being the mean light wavelength determined from emission spectra measurements as follows:

$$hc\bar{\lambda}^{-1} = hc \left\{ \int \phi_{\lambda}(\lambda)\lambda d\lambda / \int \phi_{\lambda}(\lambda) d\lambda \right\}^{-1} \quad (8)$$

where  $\phi(\lambda)$  is the scintillator's emission spectrum.

The input signal to noise ratio (SNR<sub>in</sub>) has been previously expressed, for an X-ray imaging detector, by the relation [24, 25]:

$$\text{SNR}_{\text{in}}^2 = \left( \int_0^{E_0} \phi_0(E)E dE \right)^2 / \int_0^{E_0} \phi_0(E)E^2 dE \quad (9)$$

where the numerator is equal to the square of the first statistical moment of the distribution of X-ray photons. This distribution is expressed by the X-ray spectral distribution of  $\phi_0(E)$  [27–29]. This is also equal to the square of the total incident X-ray energy fluence (input signal). The denominator is equal to the second moment of the aforementioned distribution. This second moment has been considered to express the input quantum noise. Relation (9) is used for energy integrating detectors, i.e., the detector's output signal is proportional to the X-ray energy fluence [26–28].  $\phi_0(E)$  in relation (7) was determined using a tungsten anode X-ray spectrum model [28, 29], the incident X-ray exposure measurements and the exposure to photon fluence conversion formula (see relation (A2) in appendix) [27, 28].

Finally DQE may be expressed in terms of quantities that can be experimentally determined:

$$\eta_{\text{D}}(\nu) = \frac{[\eta_{\Lambda} X]^2}{(hc/\bar{\lambda})^2 W(E_0, 0)} \frac{1}{[N^2(E_0, \nu)]} \left[ \frac{[\int \phi_0(E)E dE]^2}{\int \phi_0(E)E^2 dE} \right]^{-1} \quad (10)$$

where  $W(E_0, 0)$  is the zero frequency noise power or the limit of the noise power spectrum as frequency tends to zero,  $N(E_0, \nu)$  is the noise transfer function (NTF) defined as the ratio  $N^2(E_0, \nu) = W(E_0, \nu)/W(E_0, 0)$ .

## 2.4 Experiments

The absolute efficiency and imaging parameters were determined as follows:

1. *Preparation of scintillating screens:* The scintillating screens were prepared in our laboratory by sedimentation of the phosphor powder (code: QMK58/N-C1, Phosphor Technology Ltd. or P-56 phosphor) on fused silica substrates (spectrosil B). The density of this material was 4.15 g ml<sup>-1</sup> and mean particle size 6.6 μm and quartile deviation of 0.28 (Phosphor Technology Ltd., datasheet).

Na<sub>2</sub>SiO<sub>3</sub> was used as binding material between the powder particles. The coating thickness of the screens was 12.6 mg cm<sup>-2</sup>, 33 mg cm<sup>-2</sup>, 42 mg cm<sup>-2</sup>, 62.97 mg cm<sup>-2</sup>, 107.44 mg cm<sup>-2</sup> and 166.47 mg cm<sup>-2</sup>.

2. *Measurement of absolute efficiency:* The scintillating screens were irradiated by X-rays at various tube voltages (from 50 to 130 kV) employing a Philips Optimus X-ray radiographic unit. Tube filtration was 2.5 mm Al. An additional 20-mm Al filtration was introduced in the beam to simulate beam quality (X-ray spectrum shape) alteration by an average human body.

Absolute efficiency was determined by measuring the light energy fluence emitted by the irradiated screen and dividing by the incident exposure rate measured at screen position. The experimental set-up for light energy fluence measurements comprised a photomultiplier (EMI 9798 B) with an extended sensitivity S-20 photocathode and enclosed within a bronze light tight chamber. The photomultiplier current was amplified and fed to a vibrating reed (Cary 400) electrometer operated in current mode. An analogue to digital converter was employed to digitise electrometer's output, which was then stored on a computer. Two modes of absolute efficiency measurements were followed: (a) The transmission mode, where light emitted from the rear, not irradiated, screen side was measured and (b) The reflection mode, where light fluence emitted from the front, irradiated, side was measured. Reflection mode simulates the back screen of ordinary conventional radiographic cassettes and the conventional mammographic cassettes. Transmission mode simulates all the other types of X-ray radiographic, fluoroscopic and computed tomography detectors.

Incident exposure rate measurements were performed using a Radcal 2026C ionization chamber dosimeter (Radcal Corp. USA). Exposure rate values ranged from 4.06 mR s at 50 kV up to some decades of mR s at tube voltages higher than 100 kV.

Absolute efficiency was then computed from electrometer's output current and dosimeter data by performing conversions and corrections according to the formula:

$$\eta_{\Lambda} = \frac{i_{\text{elec}}(\text{pA})}{S n_{\text{p}} c_{\text{s}} c_{\text{g}}} \left( \frac{1}{X} \right) \quad (11)$$

where:  $i_{\text{elec}}$  is the electrometer's output current in pA.  $S$  is the area of the irradiated screen.  $n_{\text{p}}$  is the photocathode's peak photosensitivity expressed in mA/W. This was used as a factor for converting the output photocathode current into light power (light energy fluence).  $c_{\text{s}}$  is the spectral compatibility factor expressing the compatibility of the scintillator's emission spectrum to the spectral sensitivity of the photocathode (extended S-20) [15].  $c_{\text{s}}$  was determined by the relation:

$$c_{\text{s}} = \int \phi(\lambda)s(\lambda) d\lambda / \int s(\lambda) d\lambda \quad (12)$$

where  $\phi(\lambda)$  is the scintillator's emission spectrum and  $s(\lambda)$  is the spectral sensitivity of the photocathode (known from manufacturer's datasheet). This sensitivity was also verified in our laboratory using a series of prototype LED light sources (Kingbright Co) ranging from violet to red colour. The scintillator optical emission spectrum was measured during

X-ray irradiation by an Ocean Optics S2000 grating spectrometer (Ocean Optics Inc) [15].  $c_g$  is the geometric light collection efficiency of the experimental set-up expressing the fraction of screen's light incident on the photocathode. This fraction has been determined by considering: a) The angular distribution of light emitted by the screen and b) The distance between the screen and the photocathode.  $X$  is the measured incident X-ray exposure rate. According to formula (9) AE was finally expressed in units of  $\mu\text{W m}^{-1}/\text{mR s}^{-1}$ , where  $\mu\text{W m}^{-2}$  corresponds to the light flux ( $\Psi_\Lambda$ ) and  $\text{mR s}^{-1}$  to exposure rate. For simplicity the notation efficiency unit (EU) was used ( $1 \text{ EU} = \mu\text{W m}^{-1}/\text{mR s}^{-1}$ ) [16].

**MTF and NPS:** The modulation transfer function and the noise power spectrum were determined by the following techniques, which have been explicitly described in previous studies [19–21, 23]. For MTF determination the screens were used in combination with the Agfa Ortho CP-G plus radiographic film and an MTF lead test pattern (typ-53 of Nuclear Associates). The images of the MTF test pattern obtained on the film, after X-ray excitation of the screens, were digitised and processed [20]. Prior to digitisation it was verified that the film optical density values were within the linear part of the H&D characteristic curve. For the determination of the noise power spectrum, the screen-film systems were uniformly irradiated by X-rays; however, no test pattern was used. The noise power spectrum may be experimentally obtained by Fourier transforming the auto-correlation function expressing the importance of the optical density fluctuations obtained on the film after uniform screen irradiation [19, 23]. For both MTF and NPS determination the X-ray exposure was 13.03 mR.

### 3 Results and discussion

Figure 1 shows the variation of absolute efficiency of  $\text{Y}_3\text{Al}_5\text{O}_{12}:\text{Ce}$  screens with X-ray tube voltage in the range from 50 to 130 kVp. Data presented in this figure were obtained in transmission mode of measurements. Transmission mode data will be preferably shown in the next figures, since they are more appropriate to simulate modern digital detectors configuration [1–3]. Depending on X-ray tube voltage

and screen coating thickness reflection mode values were 20–30% higher than the corresponding transmission ones. The difference between reflection and transmission mode values was found maximum (34%) at 50 kVp for the  $107 \text{ mg cm}^{-2}$ . In both transmission and reflection modes the absolute efficiency of thick screens ( $107$  and  $166 \text{ mg cm}^{-2}$ ) was found to decrease continuously with increasing tube voltage. Thinner screens ( $13$ – $63 \text{ mg cm}^{-2}$ ) showed a very slow variation with increasing voltage. The highest absolute efficiency values were observed for the  $107 \text{ mg cm}^{-2}$  screen. The screen of  $166 \text{ mg cm}^{-2}$  was also found with high efficiency; however, it was slightly lower than that of the  $107 \text{ mg/cm}^2$  screen. The shape of the absolute efficiency curves is significantly affected by the corresponding X-ray energy absorption efficiency, shown in Fig. 2. This efficiency expresses strictly the fraction of incident radiation energy that is locally deposited at the point of primary photon interaction (see appendix). All other types of secondary radiation, e.g., scattered,  $K$  or  $L$ -fluorescence and bremsstrahlung, are excluded from the calculations by definition [30, 31]. Hence only the useful energy for image formation is taken into account. The curve was calculated by assuming exponential X-ray absorption, governed by the screen thickness and the X-ray mass energy absorption coefficient, as shown in the appendix (relation (A3)). The values of the energy absorption coefficient of  $\text{YAG}:\text{Ce}$  scintillator were calculated from tabulated data on absorption coefficients of yttrium, aluminum and oxygen [30, 31]. At low X-ray tube voltages thick screens ( $107 \text{ mg/cm}^2$ ) absorb relatively large fractions of incident X-ray energy (e.g., 0.29 at 50 kVp in Fig. 2), which is converted into light energy, and thus absolute efficiency increases. At higher voltages X-ray photons are more penetrating and X-ray energy absorption is lower (e.g., 0.17 at 80 kVp and 0.13 at 100 kVp for the  $107 \text{ mg/cm}^2$  screen (Fig. 2)). As a result lower light yield and lower absolute efficiency values were obtained. Concerning thin screens, the corresponding absolute efficiency curves showed very slight variation, due to their low X-ray energy absorption even at low voltages.

Figure 3 is a plot of absolute efficiency variation with screen coating thickness. Maximum absolute efficiency values

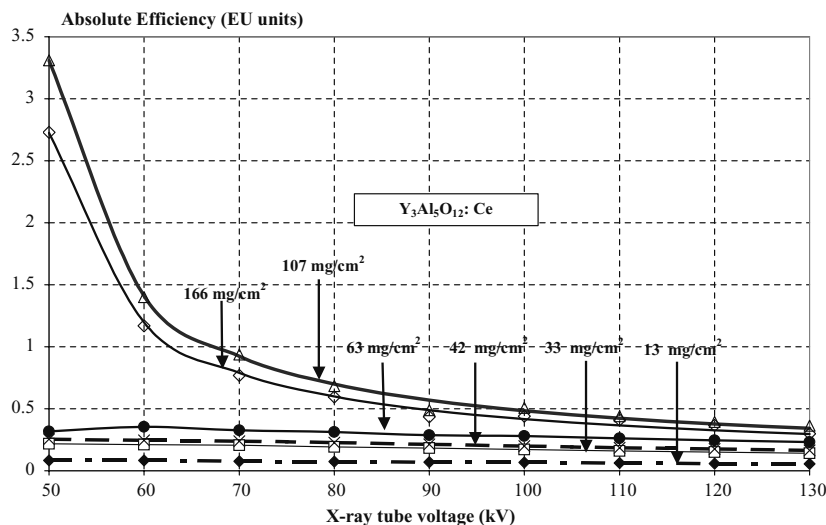


**FIGURE 1** Variation of absolute efficiency of  $\text{Y}_3\text{Al}_5\text{O}_{12}:\text{Ce}$  powder scintillating screens with increasing X-ray tube voltage. AE is expressed in absolute efficiency units (EU,  $1 \text{ EU} = \mu\text{W m}^{-1}/\text{mR s}$ )

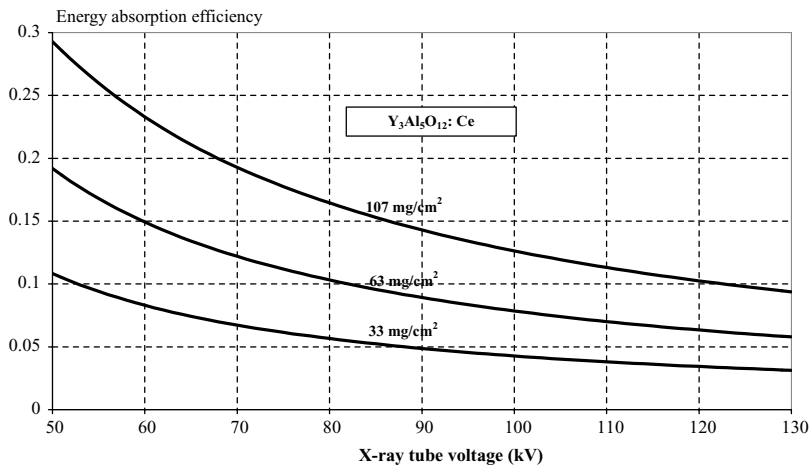


**FIGURE 2** Energy absorption efficiency of three  $Y_3Al_5O_{12}: Ce$  powder scintillating screens as a function of X-ray tube voltage

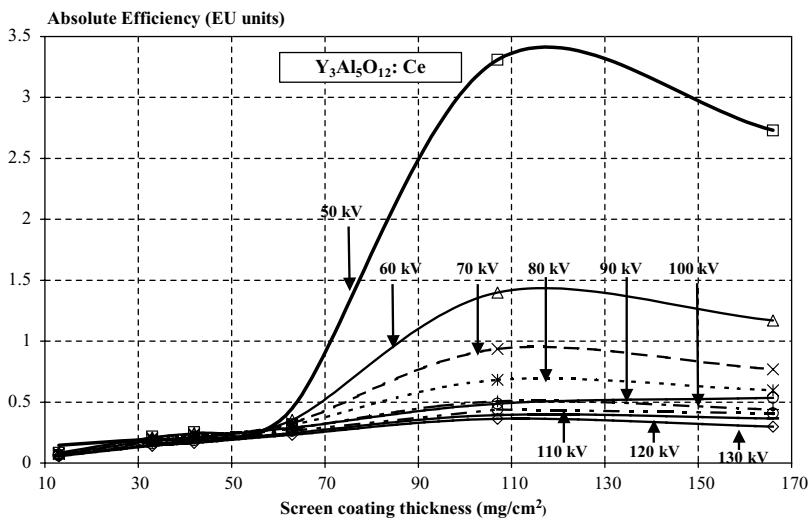


**FIGURE 3** Variation of absolute efficiency of  $Y_3Al_5O_{12}: Ce$  powder scintillating screens with increasing screen coating thickness. AE is expressed in absolute efficiency units (EU,  $1 \text{ EU} = \mu\text{W m}^{-1}/\text{mR s}$ )

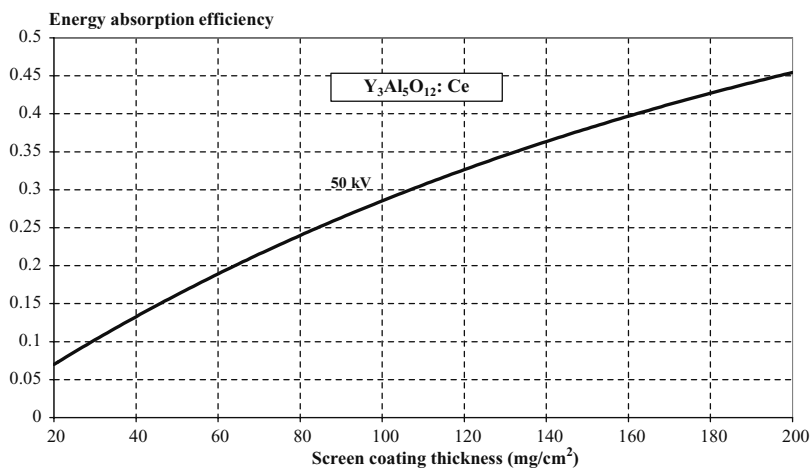


**FIGURE 4** Energy absorption efficiency of  $Y_3Al_5O_{12}: Ce$  powder scintillating screens as a function of screen coating thickness at 50 kV

were obtained for the  $107 \text{ mg cm}^{-2}$  screen for all X-ray tube voltages. For higher thicknesses, absolute efficiency shows a tendency to decrease. This may be assessed by taking into account that the values corresponding to the  $166 \text{ mg cm}^{-2}$  screen are always lower than those of the  $107 \text{ mg cm}^{-2}$  screen. The shape of these curves resulted from the combined effects of X-ray absorption and light attenuation within the phosphor mass. X-ray energy absorption increased approximately expo-

nentially with increasing coating thickness (Fig. 4). However only a small fraction ( $\eta_C$ ) of this energy is converted into light. In addition, due multiple scattering effects on phosphor grains and increased light absorption due to the elongation of photon trajectories within thick screens, this light is highly attenuated. These effects are responsible for the slightly lower efficiency of the  $166 \text{ mg/cm}^2$  with respect to that of the  $107 \text{ mg/cm}^2$  screen.

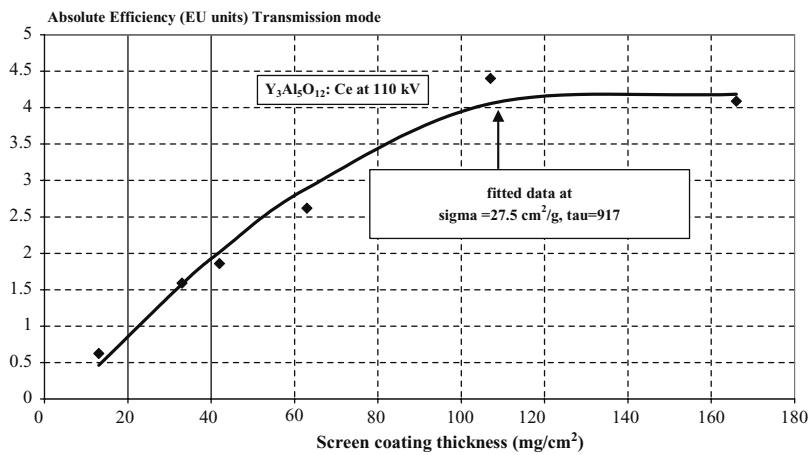


Figure 5 shows a calculated absolute efficiency curve fitted to experimental data. This curve was derived by a theoretical model based on the Hamaker-Ludwig and Swank theories [17, 18] (see appendix). This model was formulated using the relation  $\eta_A = \Psi_\Lambda / X$ , where the emitted light energy fluence,  $\Psi_\Lambda$ , was expressed by Eq. (1) in combination with Eqs. (A1)–(A7) (in appendix). These equations give the X-ray absorption efficiency, the intrinsic conversion efficiency and the light transmission efficiency. The incident X-ray fluence,  $\Psi_0(E)$  in Eq. (1), was expressed via X-ray spectral distribution data, which were obtained using the tungsten anode X-ray spectrum model [28, 29] also used for  $\text{SNR}_{\text{in}}$  determination (relation (9)). The final theoretical model equation was fitted to experimental data, shown as points in the same figure. Fitting was achieved employing the Trust-Region fitting algorithm incorporated in Matlab 6.5 software package [MathWorks\_Inc, MA, USA]. The optical attenuation coefficients  $\sigma$  and  $\tau$ , (see relation (1) and (A7) in appendix), were employed as fitting parameters. Final values of  $\sigma$  ranged from 27.1 to 28.3  $\text{cm}^2/\text{g}$  and corresponding values of  $\tau$  were 903.33–943.33  $\text{cm}^2/\text{g}$  for various X-ray tube voltages. Best fitting was obtained at 110 kVp shown in Fig. 5. The values of  $\sigma$  were close to similar values found in previous studies [14, 15], which were based on different experimental techniques. The final values of  $\sigma$  were slightly lower than those previously [20] found for rare earth scintillators ( $\sigma = 30 \text{ cm}^2/\text{g}$  for  $\text{Gd}_2\text{O}_2\text{S}$ :

Tb and  $\text{La}_2\text{O}_2\text{S}:\text{Tb}$ ) often used in ordinary radiographic detectors [1–3]. This may be explained by considering that a small fraction of the YAG:Ce emission spectrum penetrates into the higher wavelength red spectral region [15]. Since light attenuation is inversely proportional to light wavelength, the red light portion of the spectrum may affect the average value of the light attenuation coefficient. The intrinsic conversion efficiency was previously found to be approximately equal to  $\eta_C = 0.050$  [15]. Using the aforementioned values of  $\sigma$ ,  $\tau$  and  $\eta_C$ , as input data to theoretical model calculations, we estimated that the absolute efficiency of YAG:Ce scintillator becomes highest for screen coating thicknesses of 110–120  $\text{mg cm}^{-2}$ . In addition, theoretical calculations predicted that, for screens thicker than 50  $\text{mg/cm}^2$  and assuming tungsten anode X-ray spectrum, absolute efficiency peaks at 30–40 kVp.

To provide a more detailed insight into the conversion and emission properties of YAG:Ce scintillator, a comparison between the X-ray luminescence efficiency (ratio  $\Psi_\Lambda / \Psi_0$ ) and the absorbed X-ray to emitted light conversion efficiency (ECE) were plotted in Figs. 6 and 7. ECE expresses the fraction of absorbed X-ray energy that is converted into light emitted by the screen surface. ECE was defined by the product ( $\text{ECE} = \eta_C g_\Lambda(\sigma, \tau, \rho)$ ). XLE was estimated from experimental absolute efficiency values after converting the measured exposure rate, ( $\dot{X}$ ) in relation (3), into X-ray energy fluence

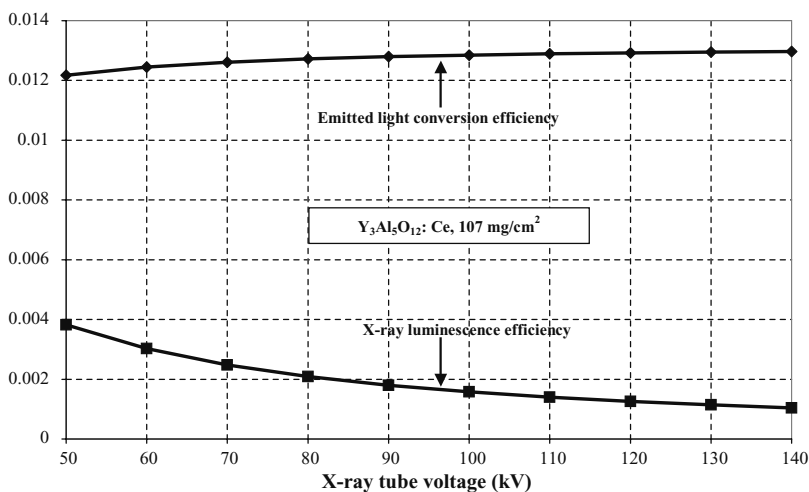
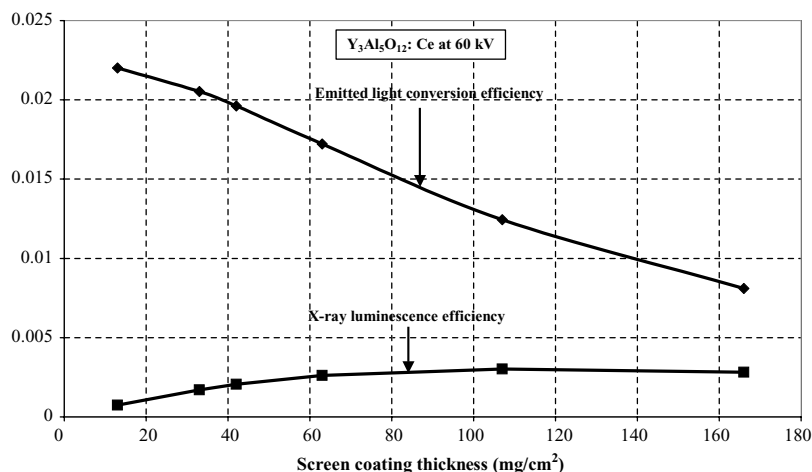


FIGURE 6 Variation of X-ray luminescence efficiency (XLE) and X-ray to emitted light conversion efficiency (ECE) with X-ray tube voltage

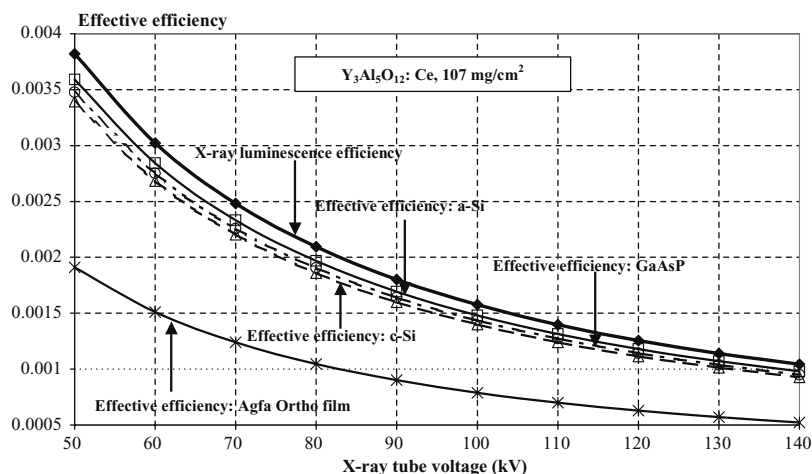


**FIGURE 7** Variation of X-ray luminescence efficiency (XLE) and X-ray to emitted light conversion efficiency (ECE) with screen coating thickness

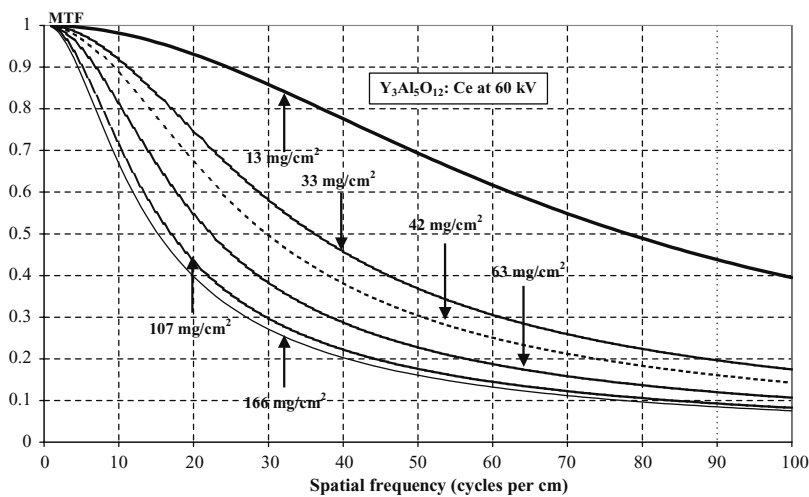
( $\Psi_0$ ). This was achieved using the corresponding conversion formula (A2) in appendix. ECE was estimated using Eqs. (A4)–(A7) in appendix. In Fig. 6 calculated curves showing XLE and ECE variation with X-ray tube voltage for the 107 mg/cm<sup>2</sup> screen are plotted. It is of interest to note that XLE (emitted light energy as a fraction of incident X-ray energy) is three to ten times lower than ECE (emitted light energy as a fraction of absorbed X-ray energy). XLE decreases from  $\eta_{\Psi} = 0.00380$ , at 50 kVp, down to  $\eta_{\Psi} = 0.00104$  at 140 kVp. This curve is of similar shape with the corresponding absolute efficiency and absorption efficiency curves (Figs. 1 and 2). On the other hand the ECE curve shows a very slight tendency to increase with increasing tube voltage, i.e., from 0.0122 at 50 kVp to 0.0129 at 140 kVp. The shape of the ECE curve is determined by the light attenuation effects while the XLE curve shape is affected by both X-ray absorption and light attenuation. Light attenuation is of lower importance at high voltages since X-ray penetration is deeper and light has to travel shorter distances through the remaining of screen mass. This is favourable for light emission in transmission mode. However at high voltages a relatively large number of X-ray photons is transmitted through the screen. Thus no energy is deposited within the scintillator mass to create light. These two effects explain the almost horizontal shape of the ECE curve. Figure 7 shows the variation of XLE and ECE with screen coating thickness at 60 kVp. XLE increases with

thickness up to a maximum value of 0.003, which is obtained in the range of 100–120 mg cm<sup>-2</sup>. ECE falls off rather fast due to the prevalence of light attenuation effects in thick screens. It should be also noted that all experimental and calculated data concerning either the absolute or the luminescence efficiency of YAG: Ce scintillator, show that the emission performance of this material is comparable to that of other yttrium based scintillators. However it was found significantly lower than that of gadolinium-based scintillators and alkali halide (CsI) scintillators [20, 21, 32]. This is to be expected since the values of a number parameters affecting detection efficiency and light generation in  $Y_3Al_5O_{12}: Ce$  scintillator, i.e.: density ( $\rho = 4.15$  g cm<sup>-3</sup>), effective atomic number ( $Z_{\text{eff}} = 23.8$ ) and energy band-gap ( $E_g = 7.01$  eV) [10–16] are below those corresponding to these materials.

Figure 8 shows effective luminescence efficiency data for various combinations of the YAG: Ce screens with optical sensors used in medical imaging systems (i.e., amorphous silicon photodiodes, crystalline silicon photodiodes, CCD arrays etc). As it may be seen a YAG: Ce scintillator based detector is of highest efficiency when YAG:Ce is combined with amorphous silicon photodiodes or CCD arrays. On the other hand YAG: Ce shows low compatibility when combined with the orthochromatic film. These results are indicative that YAG: Ce can be suitable for use in digital imaging detectors.



**FIGURE 8** Effective luminescence efficiency of  $Y_3Al_5O_{12}: Ce$  powder scintillating screens



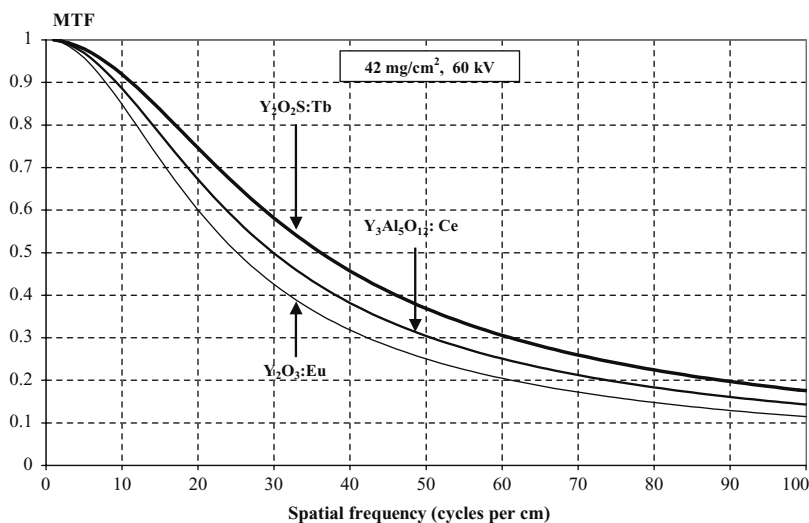
**FIGURE 9** Modulation transfer function of  $\text{Y}_3\text{Al}_5\text{O}_{12}:\text{Ce}$  screens determined at 60 kVp

Figure 9, shows the modulation transfer function of YAG: Ce screens determined at 60 kVp. MTF curves decreased with increasing screen thickness indicating that MTF is not seriously affected by the X-ray absorption properties of the scintillator. This is in accordance with the definition of MTF (relations (2), (5)) where both numerator and denominator depend on the quantum detection efficiency ( $\eta_Q$ ) of the screen. This is also the case for the light generation ( $\eta_C$ ) scintillator properties. MTF is principally affected by the directivity of light generation and the light attenuation effects (scattering and absorption), e.g., the fraction of laterally directed optical photons that arrive at the screen's emissive surface. These photons spread out on the screen surface and cause image quality degradation. The amount of these photons depends on the thickness of the screen and on the corresponding light attenuation (light absorption and light scattering) properties of the scintillator material. Thick screens prepared from scintillators of low light attenuation coefficients, although exhibiting high absolute efficiency, cause MTF degradation due to significant light spread effects. To clarify the effect of light attenuation a comparison between MTF curves corresponding to yttrium based scintillators (YAG: Ce, YOS: Tb,  $\text{Y}_2\text{O}_3:\text{Eu}$ ) is shown in Fig. 10.  $\text{Y}_2\text{O}_2\text{S}:\text{Tb}$ , corresponding to  $\sigma = 30 \text{ cm}^2/\text{g}$ , was found with higher MTF than YAG: Ce ( $\sigma = 28 \text{ cm}^2/\text{g}$ ), which

in turn was found with higher MTF than that of  $\text{Y}_2\text{O}_3:\text{Eu}$  ( $\sigma = 25 \text{ cm}^2/\text{g}$ ).

The zero-frequency normalized noise power spectrum or noise transfer function (NTF) of the YAG: Ce screens is plotted in Fig. 11. As it is observed thin screens show higher NTF curves within the whole spatial frequency range. The shape of curves is very similar to that of MTF curves.

Figure 12 is a plot of the frequency dependent DQE of the YAG: Ce screens determined at 60 kVp. In the region of low spatial frequencies, lower than  $20 \text{ cm}^{-1}$ , the screens of  $107 \text{ mg cm}^{-2}$  and  $166 \text{ mg cm}^{-2}$  showed higher DQE than thin screens. This is because the values of DQE at low frequencies are mainly affected by the ratio of the output signal, i.e. the emitted light fluence incorporated in absolute efficiency ( $\eta_A$ ), over the zero-frequency noise power (corresponding to the variance in light fluence fluctuations). This may be seen from relation (10). Since absolute efficiency is relatively high for thick screens ( $107\text{--}166 \text{ mg cm}^{-2}$ ), this explains the high DQE values of thick screens at low frequencies. As frequency increases, the DQE of the  $107$  and  $166 \text{ mg cm}^{-2}$  screens fall off faster than that of the other screens. Thus in the range of medium and high frequencies, thin screens showed slightly higher DQE values. This is due to the very fast decrease of the MTF of thick screens



**FIGURE 10** Modulation transfer function of yttrium based scintillators (YAG: Ce, YOS: Tb,  $\text{Y}_2\text{O}_3:\text{Eu}$ )

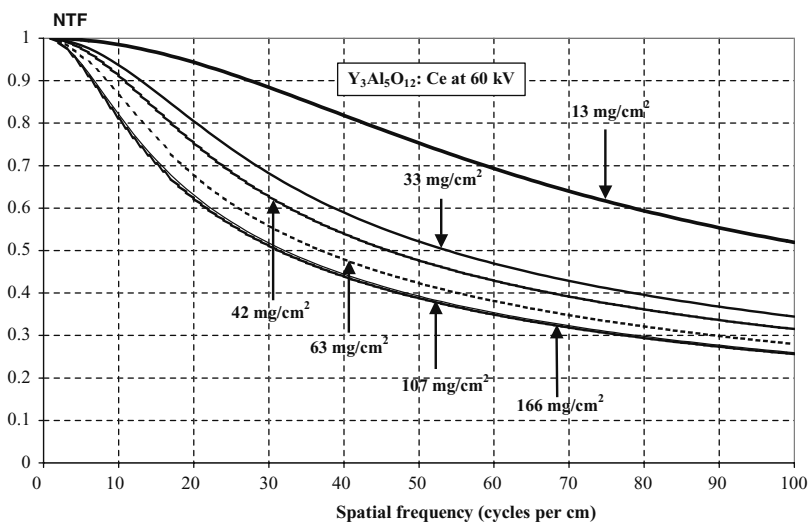


FIGURE 11 Noise transfer function (NTF) of  $Y_3Al_5O_{12}:Ce$  screens

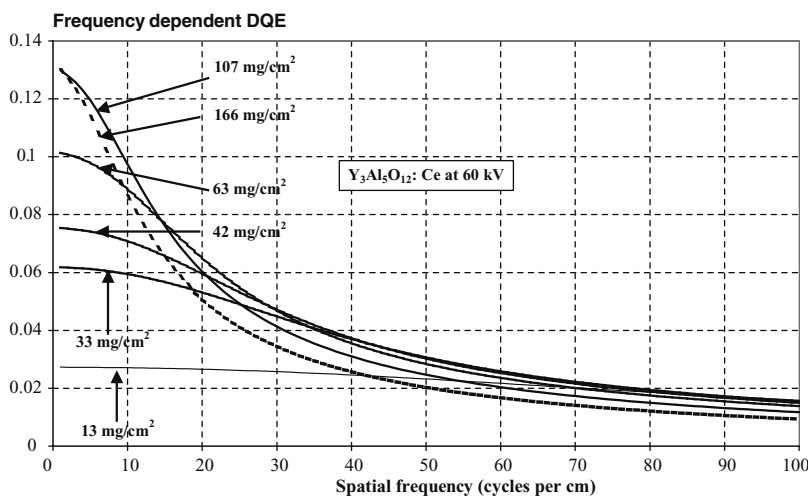


FIGURE 12 Detective quantum efficiency of  $Y_3Al_5O_{12}:Ce$  screens determined at 60 kVp

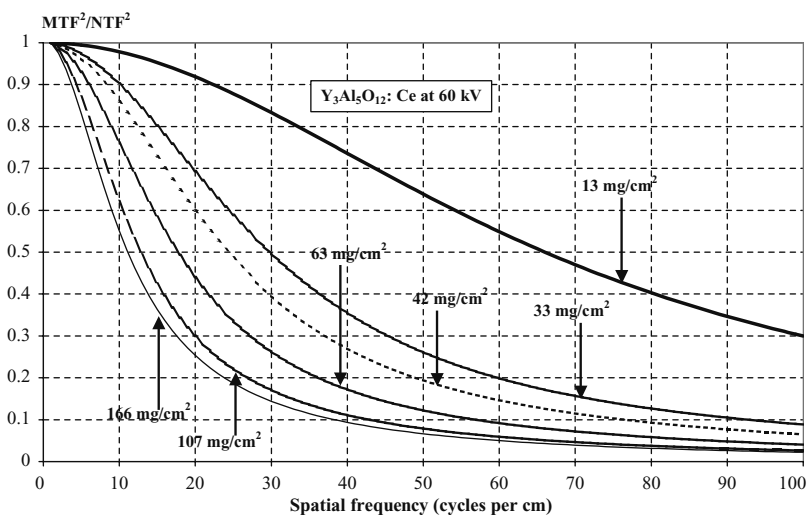


FIGURE 13 Plot of the ratio  $MTF^2(\nu)/NTF^2(\nu)$  for various  $Y_3Al_5O_{12}:Ce$  screens

within this frequency range (see Fig. 9). It has been also found that the corresponding ratio  $M^2(\nu)/N^2(\nu)$  (square of the modulation transfer function over the noise transfer function) decreases very rapidly with spatial frequency for thick screens (Fig. 13). These results are in accordance with the well-established property of screens of finite thickness where quantum noise is being passed more effectively than signal (X-ray and light fluence) through the superimposed thin

screen layers [33]. This has been previously [34] explained by taking into account that the overall screen MTF is given by the weighted sum of the separate MTFs of the elementary thin screen layers the screen is considered to consist of (see appendix A5–A6). On the other hand, NPS has been expressed as the weighted sum of the squared MTFs of the thin layers. Considering that in the quotient  $(M^2(\nu)/N^2(\nu))$  the terms are very small in value, it can be easily shown

that the MTF squared ( $M^2(\nu)$ ) is always lower than  $N^2(E_0, \nu) = W(E_0, \nu)/W(E_0, 0)$ .

#### 4 Summary and conclusion

In the present study, the absolute luminescence efficiency, the modulation transfer function and the detective quantum efficiency of  $Y_3Al_5O_{12}:Ce$  powder scintillator screens were investigated. The latter were prepared in our laboratory with various thicknesses. Measurements were obtained under conditions employed in diagnostic radiology. Peak absolute efficiency was obtained for the  $107 \text{ mg/cm}^2$  layer at low X-ray tube voltages. The overall light emission efficiency and imaging performance of YAG: Ce powder scintillator, were found comparable to other yttrium based scintillators and lower to currently employed rare earth and alkali halide scintillator materials [35]. However, taking into account its spectral compatibility to optical sensors (effective efficiency) and its very fast response, this scintillator could be considered for applications in X-ray imaging. Specifically, novel imaging techniques requiring low X-ray energies and fast response times, such as digital mammography detectors for use in computed tomography breast imaging [36] or low energy synchrotron radiation imaging systems [37] could be probable candidates.

#### Appendix

##### Incident X-ray radiation

The incident X-ray energy fluence  $\Psi_0$  and the incident X-ray photon fluence  $\Phi_0$  may be determined from exposure ( $X$ ) measurements using the relations [27, 28]:

$$\bar{\Psi}_0 = X \int_0^{kV} \frac{(\bar{W}/e)[\psi_0(E)]}{(\mu_{en}(E)/\rho)_{air}} dE / \int_0^{E_0} \psi_0(E) dE \quad (A1)$$

$$\bar{\Phi}_0 = X \int_0^{kV} \frac{(\bar{W}/e)[\phi_0(E)]}{E(\mu_{en}(E)/\rho)_{air}} dE / \int_0^{E_0} \phi_0(E) dE \quad (A2)$$

where  $\phi_0(E)$ ,  $\psi_0(E)$  denote the X-ray photon fluence and X-ray energy fluence spectral distributions respectively [27–29].  $\bar{W}$  is the mean energy required to create an electron-ion pair in air and  $(\mu_{en}(E)/\rho)_{air}$  is the total mass energy absorption coefficient for air.

##### X-ray absorption and detection efficiency

The X-ray energy absorption efficiency ( $\eta_e$ ) is given by the following relation

$$\eta_e = \frac{\int_0^{E_0} \psi_0(E) \left( \frac{\mu_{tot,en}(E)/\rho}{\mu_{tot,t}(E)/\rho} \right) (1 - e^{-(\mu_{tot,t}(E)/\rho)w}) dE}{\int_0^{E_0} \psi_0(E) dE} \quad (A3)$$

$\mu_{tot,en}$  is the total mass energy absorption coefficient of the scintillator, which includes all mechanisms of energy deposition locally at the point of primary X-ray interaction within scintillator's mass. The effect of scattered,  $K$  or  $L$ -fluorescence, and bremsstrahlung photon, are not in-

cluded [28, 30, 31].  $(\mu_{tot,t}(E)/\rho)$  is the total mass X-ray attenuation coefficient of the scintillator [28, 30, 31]. The quantum detection efficiency ( $\eta_Q$ ) may be obtained after replacing the X-ray energy fluence ( $\psi_0$ ) by the X-ray photon fluence ( $\phi_0$ ) and the total mass energy absorption coefficient ( $\mu_{tot,en}(E)/\rho$ ) by the total mass attenuation coefficient ( $\mu_{tot,t}(E)/\rho$ ) [30, 31].

##### The intrinsic conversion efficiency

The intrinsic conversion efficiency was calculated by the Eq. [1, 4, 6, 15]:

$$\eta_C = (hc/\bar{\lambda})/\beta E_g \quad (A4)$$

where  $hc/\bar{\lambda}$  is the average energy of emitted light photons.  $\beta E_g$  represents the average energy that must be transferred by a fast electron (e.g., a photoelectron) to create an electron-hole pair in the scintillator material.  $E_g$  is the forbidden energy band-gap between the valence and the conduction energy bands of the scintillator material [1, 4, 5, 11].  $\beta$  is a parameter related to energy losses to lattice vibrations. For  $Y_3Al_5O_{12}$  scintillator,  $\beta = 5.6$  and  $E_g = 7.01 \text{ eV}$  [5, 6, 10].

##### The light transmission efficiency

The light transmission efficiency,  $\bar{g}_\Lambda(\sigma, \tau, \rho)$  in relations (1) and (2), of a scintillating screen may be expressed as follows:

$$g_\Lambda(E, \sigma, \tau, \rho) = \int_0^{w_0} \bar{\varphi}_X(E, w) \bar{g}_\Lambda(\sigma, \tau, \rho, w) dw dE \quad (A5)$$

$w_0$  is the total screen thickness. For the purposes of analysis it has been considered that the screen was divided into a large number of superimposed elementary thin layers of thickness  $\Delta w$ . Here  $w$  denotes the depth of each thin layer from the screen surface. The function  $\bar{\varphi}_X(E, w)$  describes the relative probability of X-ray absorption at a depth  $w$  from the screen surface by the relation:

$$\bar{\varphi}_X(E, w) = \frac{\mu(E) \exp[-\mu(E)w] dw}{\int_0^{w_0} \mu(E) \exp[-\mu(E)w] dw} \quad (A6)$$

where  $\mu(E)$  is the X-ray absorption coefficient calculated using tabulated data [30, 31]. The numerator in Eq. (A6) gives the probability of X-ray photon absorption at depth  $w$ . The denominator is equal to the total probability of absorption in a scintillator of thickness  $w_0$ .

The function  $\bar{g}_\Lambda(\sigma, \tau, \rho)$  has been defined as a solution to the photon diffusion differential Eq. [17, 18] describing light propagation through light scattering media:

$$\begin{aligned} \bar{g}_\Lambda(\sigma, \tau, \rho) &= \frac{\tau \rho_1 [(\sigma + \tau \rho_0) e^{\sigma w} + (\sigma - \tau \rho_0) e^{-\sigma w}]}{(\sigma + \tau \rho_0)(\sigma + \tau \rho_1) e^{\sigma w_0} - (\sigma - \tau \rho_0)(\sigma - \tau \rho_1) e^{-\sigma w_0}} \end{aligned} \quad (A7)$$

where  $\sigma$  is the light attenuation coefficient of the scintillator, which is equal to the reciprocal of the light photon diffusion length [13, 17, 18], and it is given as a function of the optical scattering coefficient ( $s$ ), and the optical absorption coefficient

( $a$ ), i.e.,  $\sigma = [a(a + 2s)]^{1/2}$ . In the spatial frequency domain,  $\sigma$  is written as  $\sigma = \sigma_0^2 + 4\pi\nu^2$ , where  $\sigma_0$  corresponds to zero-frequency [18].  $\tau$  is the inverse relaxation length given as  $\tau = a + 2s$ .  $\rho_0$ ,  $\rho_1$  are optical parameters expressing the reflection of light at the front and back scintillator surfaces:  $\rho_n = (1 - r_n)/(1 + r_n)$ , where  $r_n$  denotes the optical reflection coefficients at the front ( $n = 0$ ) and back ( $n = 1$ ) screen surfaces. In this study we have used  $\rho_0 = 0.91$ ,  $\rho_1 = 0.87$  (obtained from previous studies [16, 18, 20, 23]) and the values of  $\sigma$  and  $\tau$  found by fitting (see text). Eq. (A7) corresponds to transmission mode. To describe reflection mode emission the coating thickness,  $w$  in Eq. (A7), was replaced by  $(w_0 - w)$ .

**ACKNOWLEDGEMENTS** This study was financially supported through the research programme EPEAEK “Archimidis”.

## REFERENCES

- H. Wiczorek, *Rad. Meas.* **33**, 541 (2001)
- J.A. Rowlands, J. Yorkston, in *Handbook of Medical Imaging, vol. 1, Physics and Psychophysics*, ed. by J. Beutel, H.L. Kundel, R.L. Van Metter (SPIE Press, Bellingham, 2000), pp. 234–248
- C.W.E. van Eijk, *Phys. Med. Biol.* **47**, R85–R106 (2002)
- G. Blasse, B.C. Grabmaier, *Luminescent Materials* (Springer-Verlag, Berlin, Heidelberg, 1994) p. 85
- C.W.E. van Eijk, *Nucl. Instr. Meth. Phys. Res. A* **460**, 1 (2001)
- G. Blasse, *J. Luminescence*, **60&61**, 930 (1994)
- T. Kano, in *Phosphor Handbook*, ed. by S. Shionoya, W.M. Yen (CRC Press, Boca Raton, 1999), pp. 177–186
- E. Zych, C. Brecher, *J. Alloys. Compounds* **300–301**, 495 (2000)
- M. Grinberg, A. Sikorska, S. Kaczmarek, *J. Alloys. Compounds* **300–301**, 158 (2000)
- T. Ludziejewski, M. Moszynski, M. Kapusta, D. Wolski, W. Klamra, K. Moszynska, *Nucl. Instrum. Meth. Phys. Res. A* **398**, 287 (1997)
- E. Zych, C. Brecher, J. Glodo, *J. Phys. Condens. Matter* **12**, 1947 (2000)
- E. Zych, C. Brecher, A.J. Wojtowicz, H. Lingertat, *J. Luminescence* **75**, 193 (1997)
- R. Mueller-Mach, G.O. Mueller, M.R. Kramers, T. Trottier, *IEEE J.Sel. Top. Quantum Electron.* **8**, 339 (2002)
- A. Baciero, L. Placentino, K.J. Mc Carthy, L.R. Barquero, A. Ibarra, B. Zurro, *J. Appl. Phys.* **85**, 6790 (1999)
- I. Kandarakis, D. Cavouras, I. Sianoudis, et al, *Nucl. Instrum. Meth. Phys. Res. A* **538**, 615 (2005)
- D. Cavouras, I. Kandarakis, C.D. Nomicos, A. Bakas, G.S. Panayiotakis, *Rad. Meas.* **32**, 5 (2000)
- G.W. Ludwig, *J. Electrochem. Soc.* **118**, 1152 (1971)
- R.K. Swank, *Appl. Opt.* **12**, 1865 (1973)
- I. Kandarakis, D. Cavouras, G.S. Panayiotakis, C.D. Nomicos, *Appl. Phys. B* **72**, 877 (2001)
- I. Kandarakis, D. Cavouras, *Eur. Radiol.* **11**, 1083 (2001)
- D. Cavouras, I. Kandarakis, T. Maris, G.S. Panayiotakis, C.D. Nomicos, *Appl. Phys. A* **72**, 67 (2000)
- J.C. Dainty, R. Shaw, *Image Science* (Academic Press, New York, 1974) pp 232–380
- N. Kalivas, E. Costaridou, I. Kandarakis, D. Cavouras, C.D. Nomicos, G.S. Panayiotakis, *Nucl. Instrum. Meth. Phys. Res. A* **490**, 614 (2002)
- G. Borasi, A. Nitrosi, P. Ferrari, D. Tassoni, *Med. Phys.* **30**, 1719 (2003)
- E. Samei, M.J. Flynn, *Med. Phys.* **29**, 447 (2002)
- I.A. Cunningham, in *Handbook of Medical Imaging, vol. 1, Physics and Psychophysics*, ed. by J. Beutel, H.L. Kundel, R.L. Van Metter (SPIE Press, Bellingham, 2000), pp. 82–156
- J.R. Greening, *Fundamentals of Radiation Dosimetry* (Institute of Physics, London, 1985) pp. 35–59
- J.M. Boone, in *Handbook of Medical Imaging, vol. 1, Physics and Psychophysics*, ed. J. Beutel, H.L. Kundel, R.L. Van Metter (SPIE Press, Bellingham, 2000) pp. 36–57
- J.M. Boone, J.A. Seibert, *Med. Phys.* **24**, 1661 (1997)
- J.H. Hubbel, S.M. Seltzer, *Tables of X-ray Mass Attenuation Coefficients and Mass Energy Absorption Coefficients 1 keV to 20 MeV for Elements Z = 1 to 92 and 48 Additional Substances of Dosimetric Interest*. U.S. Department of Commerce. NISTIR 5632, 1995
- E. Storm, H. Israel, *Photon Cross-Sections from 0.001 to 100 MeV for Elements 1 Through 100 Report LA-3753*, Los Alamos Scientific Laboratory of the University of California, 1967
- D. Cavouras, I. Kandarakis, A. Bakas, D. Triantis, C.D. Nomicos, G.S. Panayiotakis, *Brit. J. Radiol.* **71**, 766 (1998)
- G. Lubberts, *J. Opt. Soc. Am.* **58**, 1475 (1968)
- R.M. Nishikawa, M.J. Yaffe, *Med. Phys.* **17**, 894 (1990)
- P.R. Granfors, R. Aufrichtig, G.E. Possin, B.W. Giambattista, Z.S. Huang, J. Liu, B. Ma, *Med. Phys.* **30**, 2715 (2003)
- B. Chen, R. Ning, *Med. Phys.* **29**, 755 (2002)
- A. Gorin, K. Kuroda, I. Manuilov, A. Riazantsev, T. Ishikawa, H. Kamitsubo, M. Suzuki, H. Toyokawa, *Nucl. Instr. Meth. Phys. Res A* **510**, 76 (2003)